



Cite this: *RSC Adv.*, 2019, 9, 38973

# NO reduction over an Al-embedded MoS<sub>2</sub> monolayer: a first-principles study†

Mehdi D. Esrafilī \* and Safa Heydari

Converting toxic air pollutants such as nitric oxide (NO) and carbon monoxide (CO) into less harmful gases remains a critical challenge for many industrial technologies. Here, by performing first-principles calculations, we introduce a cheap, stable and novel catalyst for the conversion of NO and CO molecules into N<sub>2</sub>O and CO<sub>2</sub> using Al-doped MoS<sub>2</sub> (Al–MoS<sub>2</sub>). According to our results, dissociation of NO molecules on Al–MoS<sub>2</sub> has a large energy barrier (3.62 eV), suggesting that it is impossible at ambient temperature. In contrast, the coadsorption of NO molecules to form (NO)<sub>2</sub> moieties is characterized as the first step of the NO reduction process. The formed (NO)<sub>2</sub> is unstable on Al–MoS<sub>2</sub>, and hence it is easily decomposed into N<sub>2</sub>O molecules, and an oxygen atom is adsorbed onto the Al atom (O<sub>ads</sub>). This reaction step is exothermic and needs an activation energy of 0.37 eV to be overcome. Next, the O<sub>ads</sub> moiety is removed from the Al atom by a CO molecule, and thereby the Al–MoS<sub>2</sub> catalyst is recovered for the next round of reaction. The side reaction producing NO<sub>2</sub> via the reaction of NO with the O<sub>ads</sub> moiety cannot proceed on Al–MoS<sub>2</sub> due to its large activation energy.

Received 25th July 2019  
 Accepted 13th November 2019

DOI: 10.1039/c9ra05759e

rsc.li/rsc-advances

## 1. Introduction

Air pollution originating from the burning of fossil fuels in different mobile and stationary power plants is a serious threat to human health and the environment.<sup>1</sup> Nitric oxide (NO), which accounts for more than 90% of nitrogen oxides (NO<sub>x</sub>), is a highly toxic gas emitted into the atmosphere with many negative impacts on the environment such as acid rain and photochemical smog formation, and ozone layer depletion.<sup>2</sup> Moreover, any exposure to this toxic gas can cause many devastating effects on human health. Therefore, it is desirable to develop and search for efficient approaches to reduce the atmospheric concentration of NO. The catalytic reduction of NO has gained much attention in recent years,<sup>3–7</sup> due to its high efficiency, selectivity and simplicity. Previous studies<sup>8–14</sup> have indicated that NO could be converted into N<sub>2</sub>O, N<sub>2</sub> or NO<sub>2</sub> species in the presence of CO as the reducing agent. This is promising, since it also provides a route for removing toxic CO from the atmosphere. For instance, Gopinath and co-workers<sup>15</sup> have investigated the reduction of NO by CO over the Pd(111) surface by means of molecular beam technique. First-principles calculations have also indicated that NO molecules could be easily transformed into N<sub>2</sub>O over Au(111) via a dimer mechanism.<sup>16</sup> Clearly, for large-scale applications, low cost noble-

metal free catalysts with high catalytic performance are desirable.

Recently, layered materials have attracted much scientific attention due to their diverse applications in many fields of chemistry, physics and material science.<sup>17–24</sup> Molybdenum disulfide (MoS<sub>2</sub>) is a layered material with unique properties such as chemical inertness, high chemical stability, photo-corrosion resistance and specific optical properties.<sup>25,26</sup> In addition, owing to its high specific area, MoS<sub>2</sub> can act as an ideal substrate to anchor atomically dispersed metal atoms. However, pure MoS<sub>2</sub> is chemically inert to effectively stabilize deposited metal atoms, due to the absence of any dangling bonds. Hence, further optimization of active sites is desirable to increase the overall catalytic performance of MoS<sub>2</sub>.<sup>27–29</sup> For instance, the basal plane of MoS<sub>2</sub> has been successfully activated for hydrogen evolution reaction (HER) by generating sulfur vacancies.<sup>30,31</sup> González *et al.*<sup>32</sup> have indicated that the introduction of defects in MoS<sub>2</sub> leads to a notably increase of the adsorption energy of small inorganic molecules (CO<sub>2</sub>, CO, H<sub>2</sub>O, NO, NO<sub>2</sub>, H<sub>2</sub> and N<sub>2</sub>) accompanied by a larger charge transfer. On the other hand, intensive theoretical and experimental studies<sup>33–38</sup> have proven that doping of MoS<sub>2</sub> with foreign atoms can considerably modify its surface reactivity and electronic structure. Earlier quantum chemical calculations have indicated that Fe-,<sup>39</sup> Co- or Ni-<sup>40</sup> doped MoS<sub>2</sub> exhibits distinctive catalytic activity for reduction of O<sub>2</sub> molecule. Using density functional theory (DFT) calculations and experiments, Park and coworkers<sup>41</sup> have indicated that adding cobalt (Co) clusters on MoS<sub>2</sub> can greatly catalyze the HER process. Interestingly, the highest HER activity was obtained when the metal

Department of Chemistry, Faculty of Basic Sciences, University of Maragheh, P. O. Box 55136-553, Maragheh, Iran. E-mail: esrafilī@maragheh.ac.ir; Fax: +98 4212276060; Tel: +98 4212237955

† Electronic supplementary information (ESI) available. See DOI: 10.1039/c9ra05759e



clusters are decorated over the S-vacancies with the interface of Co–Mo as the preferred active site. Recently, Li and coworkers<sup>42</sup> have found that a single Al atom supported by defective MoS<sub>2</sub> can serve as a robust and promising catalyst for oxidation of CO molecule. Apart from such outstanding catalytic activity, these metal-doped substrates show also high structural stability owing to strong binding of the metal atom to MoS<sub>2</sub>, which render them as ideal catalysts used in automotive exhausts, industrial gas streams or fuel cells.

Experimental studies and theoretical calculations have shown that a variety of structural defects could be unavoidably introduced in the MoS<sub>2</sub> monolayer.<sup>43–45</sup> S-vacancy is one of the most popular intrinsic structural defects in MoS<sub>2</sub>, which can be produced in a controllable way by low-energy argon sputtering<sup>46</sup> as well as electron irradiation<sup>47,48</sup> process. First-principle calculations have shown that the formation of S-vacancy defects in MoS<sub>2</sub> is energetically more favorable than Mo-vacancy ones.<sup>39,45</sup> A recent study<sup>49</sup> has also shown the potential of S-vacancy defective MoS<sub>2</sub> monolayers to serve as an active substrate in dissociation of H<sub>2</sub>O molecules.

While much research attention has been paid to study the adsorption behavior of chemically doped MoS<sub>2</sub> monolayer toward small gas molecules, however, as far as we know, there is still a lack of detailed information about the mechanism of NO reduction over these systems. The present study aims to investigate the reaction pathways and energy barriers for reduction of NO molecules over Al-doped MoS<sub>2</sub> (Al–MoS<sub>2</sub>) using the DFT calculations. We chose Al, since it is cheap, environmentally friendly and abundant in the Earth's crust, which meets our requirement to seek low-cost catalysts for reduction of NO. In addition, the large adsorption energy of Al atom suggests that it is tightly anchored on the vacancy site, prohibiting its diffusion over the MoS<sub>2</sub> surface. As a result, Al–MoS<sub>2</sub> is introduced as a stable catalyst for reduction of NO. According to our results, the low-temperature reduction of NO is most likely to occur over Al–MoS<sub>2</sub> due to its low energy barriers.

## 2. Computational details

The first-principles DFT calculations were carried out with the DMol<sup>3</sup> code,<sup>50,51</sup> by employing the Perdew–Burke–Ernzerhof (PBE)<sup>52</sup> density functional and a double numerical plus polarization (DNP) basis set. The relativistic effects in the Mo atoms were treated by the DFT semicore pseudopotentials (DSPPs) core method.<sup>53</sup> The weak van der Waals interactions were considered *via* the Grimme's DFT-D2 scheme.<sup>54,55</sup> The convergence threshold for self-consistent iteration in the geometry optimization was set at 10<sup>−5</sup> Ha, while the convergence criteria for the force and displacement was set to 0.001 Ha Å<sup>−1</sup> and 0.005 Å, respectively. The Monkhorst–Pack *k*-point mesh was set 3 × 3 × 1 in the geometry relaxations, while 10 × 10 × 1 in the density of states (DOS) analysis. To locate transition state structures, the complete linear synchronous transit and quadratic synchronous transit (LST/QST) method was adopted and their nature (with only one imaginary frequency) was identified by the frequency calculations. Zero point energies (ZPE) obtained from the frequency calculations were then used

to correct energy barriers. In addition, thermal correction to the energy barriers and reaction energies was also considered.

The pristine MoS<sub>2</sub> is a hexagonal layered material with the S–Mo–S sandwich layers. To model it, we employed a 5 × 5 × 1 monolayer, which involves 25 Mo and 50 S atoms. The Al–MoS<sub>2</sub> was then obtained by replacing one S atom of the pristine MoS<sub>2</sub> with a single Al atom. The interaction between the layers was avoided by setting 20 Å empty space along the *z*-direction. After the full geometry relaxation, the lattice parameters of 3.18 Å were obtained for the pristine MoS<sub>2</sub>, which are in excellent accordance with those of earlier experimental and theoretical studies.<sup>56,57</sup>

To evaluate the relative stability of Al–MoS<sub>2</sub> with respect to the pure MoS<sub>2</sub>, the formation energy ( $E_{\text{form}}$ ) was calculated as

$$E_{\text{form}} = E_{\text{Al–MoS}_2} - E_{\text{MoS}_2} + E_{\text{S}} - E_{\text{Al}} \quad (1)$$

where  $E_{\text{Al–MoS}_2}$ ,  $E_{\text{MoS}_2}$ ,  $E_{\text{S}}$  and  $E_{\text{Al}}$  is the energy of the Al–MoS<sub>2</sub>, pure MoS<sub>2</sub>, a single S atom and Al atom, respectively.

The adsorption/coadsorption energy ( $E_{\text{ads}}$ ) was obtained using the following equation:

$$E_{\text{ads}} = E_{\text{total}} - E_{\text{X}} - E_{\text{substrate}} \quad (2)$$

where  $E_{\text{total}}$  is the total energy of the adsorbate(s) + substrate configuration,  $E_{\text{X}}$  is the energy of the free adsorbate and  $E_{\text{substrate}}$  is the energy of the bare Al–MoS<sub>2</sub> substrate. Based on this equation, a negative  $E_{\text{ads}}$  value should correspond to an energetically favored adsorption or coadsorption process.

## 3. Results and discussion

### Surface properties and stability of Al–MoS<sub>2</sub>

We first examine the possibility to introduce an Al atom in the single S-vacancy of MoS<sub>2</sub>. Fig. 1 shows the optimized geometry, charge density difference map and total density of states (TDOS) plot of Al–MoS<sub>2</sub>. It is evident from Fig. 1a that Al atom is stably anchored in the vacancy site of MoS<sub>2</sub> due to the formation of three covalent bonds with the neighboring Mo atoms. The relaxed Al–Mo bond distances in Al–MoS<sub>2</sub> are 2.64 Å, which are larger than the S–Mo bond lengths in the pure MoS<sub>2</sub> (*ca.* 2.44 Å). The adsorption energy of Al atom over the vacancy site of MoS<sub>2</sub> is −3.55 eV, which is larger than the cohesive energy of the bulk Al (−3.35 eV).<sup>58</sup> This finding ensures that Al atom prefers to be adsorbed on the defective MoS<sub>2</sub> in the form of single atoms and thus the clustering of the Al atoms might be avoided. On the other hand, the formation energy ( $E_{\text{form}}$ ) of Al–MoS<sub>2</sub> is obtained as 2.57 eV, which is in excellent accordance with the value reported in the ref. 21. Considering the charge density difference map in Fig. 1b, it is seen that a quite large electron density loss area appears above Al, which indicates the potential of this atom to interact with nucleophilic species. Similarly, the Hirshfeld analysis reveals that about 0.20 |*e*| shifts from Al to the defective MoS<sub>2</sub>, and each of the three nearest Mo atoms has a positive charge of 0.18 |*e*|. Furthermore, the doping of Al atom is proven to decrease band gap of MoS<sub>2</sub> from 1.73 eV in the pure state to 0.30 eV in Al–MoS<sub>2</sub>. The latter is mainly related to the



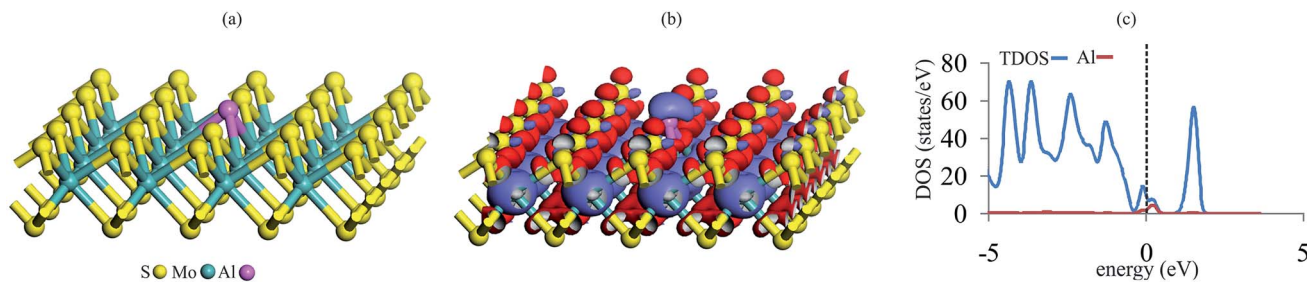


Fig. 1 (a) The relaxed geometry, (b) charge density difference and (c) TDOS/PDOS plot of Al–MoS<sub>2</sub>. The red and violet regions in charge density difference map indicate the charge loss and accumulation regions, respectively. The dashed line in the TDOS/PDOS plot indicates the Fermi level (set to be zero).

localization of impurity Al-3p states between the valence and conduction bands (Fig. 1c). Considering that a small band gap corresponds to low kinetic stability, thus it is suggested that the Al-doping significantly tunes the surface reactivity and electronic structure of MoS<sub>2</sub>. This is very important for capture and activation of NO and CO molecules, as which will be discussed in the following sections.

To further clarify the stability of the Al–MoS<sub>2</sub> substrate, we also investigate the reaction path and energy profile for the migration of the Al atom into neighboring hollow sites. Fig. S1 of ESI† represents the optimized geometry of involved stationary points in this process. Looking at Fig. S1,† one can see that the activation energy required for the migration of Al atom on MoS<sub>2</sub> is quite high (0.98 eV). This confirms our above finding that the Al atom binds tightly at the defect site of MoS<sub>2</sub>, and hence the clustering problem would be avoided. Besides, the relatively large positive reaction energy reveals that the final structure is thermodynamically less stable than the initial one. These results demonstrate that Al–MoS<sub>2</sub> would remain as a stable catalyst at normal temperatures.

### Adsorption of NO and CO molecules

After studying the surface reactivity and stability of Al–MoS<sub>2</sub>, we now focus on the catalytic activity of this substrate for NO reduction. Considering that the initial adsorption configuration of reactants on the catalyst surface plays a critical role in the subsequent reaction pathway, we first consider the most stable adsorption configurations of NO and CO molecules on the Al–MoS<sub>2</sub> substrate. Fig. 2 indicates the optimized geometries, along with the corresponding partial density of states (PDOS) and electron density difference (EDD) maps. To compare the adsorption behavior of NO and CO, adsorption energy ( $E_{\text{ads}}$ ) and net charge-transfer ( $q_{\text{CT}}$ ) values are obtained and summarized in Table 1.

Looking at Fig. 2a and b, one can see that NO molecule adsorbs onto Al–MoS<sub>2</sub> through either its N- (configuration C1) or O-site (configuration C2). For both configurations, it is found that NO adopts a linear configuration above Al atom, like as those reported on other nanostructures.<sup>7,59,60</sup> The minimum distance between NO and Al atom in C1 is 1.79 Å, which is shorter than that of C2 (1.88 Å). Moreover, comparing the  $E_{\text{ads}}$  values in Table 1 reveals that the formation of C1 configuration

is about 0.90 eV more favorable than C2. This result is in accordance with those of other reported theoretical works,<sup>61</sup> and might be ascribed to the greater contribution of the N atom in the single-occupied molecular orbital (SOMO) of NO molecule (Fig. S2†). From Table 1, it is found that the adsorption of NO is accompanied with a shift of 0.05  $|e|$  from Al–MoS<sub>2</sub> to NO, which occupy the half-filled  $2\pi^*$  orbital of NO and hence leads to an increase in the N–O bond distance. Such a favorable orbital interaction can be also understood from the PDOS plots in Fig. 2a and b, in which the 3p states of Al atom are considerably mixed with the  $2\pi^*$  states of NO around the Fermi level. Note that because of the stronger interaction, this orbital hybridization is more dominant for the configuration C1 than C2. As indicated in Fig. 2a and b, the adsorption of NO on the title surface leads to a considerable shift in the energy of NO- $2\pi^*$  states. Meanwhile, the energy of the NO- $5\sigma$  state remains almost unchanged. Besides, the corresponding EDD maps reveals that the adsorption of NO molecule induces a considerable electron density redistribution above NO molecule. In particular, a large electron density accumulation between the Al and NO in C1 implies the formation of a strong covalent Al–N bond, and hence the chemisorption of NO.

From Fig. 2c, it is found that CO is chemisorbed over the Al atom and forms an Al–C bond with a length of 1.99 Å (configuration C3). The C–O bond distance of the adsorbed CO is stretched to 1.15 Å, which is 0.01 Å larger than that of isolated CO (1.14 Å). This indicates that CO is also activated over Al–MoS<sub>2</sub> substrate. The calculated  $E_{\text{ads}}$  and  $q_{\text{CT}}$  values of CO are  $-1.34$  eV and 0.13  $|e|$ , respectively, demonstrating that it is strongly chemisorbed on the Al atom. Note that the obtained  $E_{\text{ads}}$  value is in good agreement with that of reported in the earlier study ( $-1.30$  eV).<sup>42</sup> Considering the PDOS plots, the CO adsorption onto the Al atom is mostly ascribed to the hybridization of empty Al-3p and filled CO- $5\sigma$  states around the Fermi level. Consequently, the density of states arising from the  $5\sigma$  state of adsorbed CO is smaller than that of free CO molecule. On the other hand, there also exists an orbital mixing between the Al-3p and empty CO- $2\pi^*$  orbitals, which accounts for the elongation and activation of C–O bond. This results in also a notable shift in the energy of CO- $2\pi^*$  states towards the Fermi level (Fig. 2c). These findings are supported by the EDD map in Fig. 2c, in which the chemisorption of CO onto the Al atom is



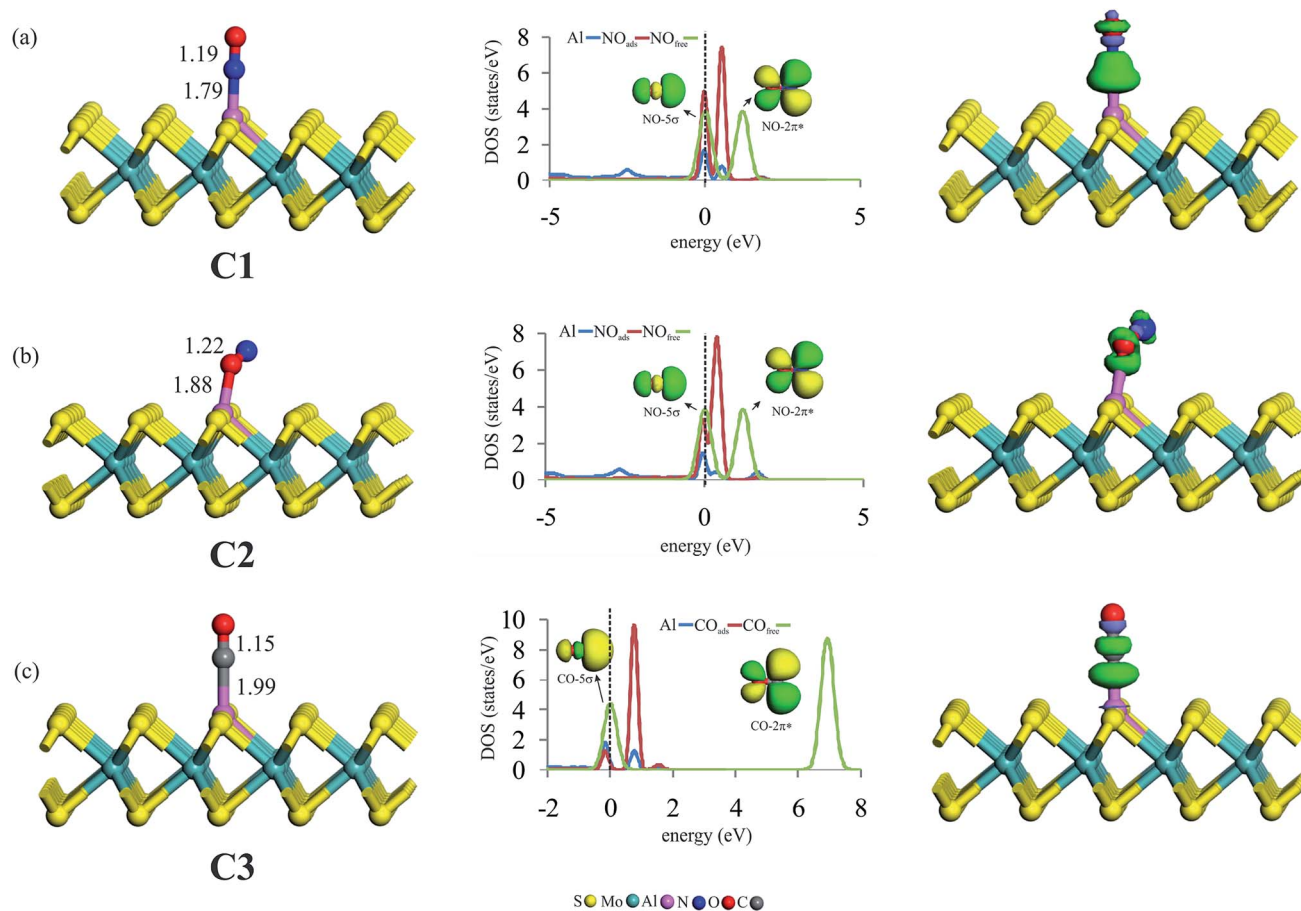


Fig. 2 The geometry configuration, PDOS and EDD plots of (a) NO, (b) ON and (c) CO adsorbed over Al–MoS<sub>2</sub>. The dashed line in the PDOS plots shows the Fermi level (set to be zero). The green and violet colors in the EDD plots indicate electron density accumulation and loss regions, respectively.

**Table 1** Adsorption/coadsorption energy ( $E_{\text{ads}}$ , eV), and net Hirshfeld charge-transfer ( $q_{\text{CT}}$ , |e|) values of the most stable configuration of NO and CO molecules on Al–MoS<sub>2</sub>

Species (configuration)	$E_{\text{ads}}$	$q_{\text{CT}}^a$
NO (C1)	−1.92	−0.06
NO (C2)	−1.01	−0.05
CO (C3)	−1.34	+0.13
2NO (D1)	−4.71	−0.52
2NO (D2)	−3.55	−0.44

<sup>a</sup> A positive  $q_{\text{CT}}$  value indicates the charge-transfer from the adsorbate to the surface, while a negative  $q_{\text{CT}}$  value indicates the charge-transfer from the surface to the adsorbate.

characterized by a large electron density redistribution on the interacting moieties. Interestingly, the depletion of electron density between the C and O atoms of CO verifies the charge-transfer from the substrate to the CO-2 $\pi^*$  orbital. Noteworthy is that the  $E_{\text{ads}}$  value for the adsorption of CO (configuration C3) is less than that of NO (configuration C1), suggesting that the tendency of Al–MoS<sub>2</sub> to capture CO molecule is lower than NO. That is, in the presence of a CO/NO mixture as a reaction gas,

the active site of the catalyst (*i.e.*, Al atom) would be covered by NO molecules. Hence, the CO poisoning of Al–MoS<sub>2</sub> would be avoided.

### Reaction mechanisms of NO reduction

To study the potential of Al–MoS<sub>2</sub> as a catalyst for reduction of NO to N<sub>2</sub>O, both the well-known “direct dissociation” and “dimer” mechanisms are investigated.<sup>61</sup> The former mechanism involves dissociation of NO molecule into N<sub>ads</sub> and O<sub>ads</sub> species, both adsorbed onto the catalyst surface. After that, the second NO attacks the N<sub>ads</sub> to yield N<sub>2</sub>O molecule. On the other hand, NO molecule in the dimer mechanism is attached to the pre-adsorbed NO to produce (NO)<sub>2</sub> species, which its subsequent dissociation results in N<sub>2</sub>O and O<sub>ads</sub> moieties. Fig. 3–6 show the optimized stationary points on the potential energy surfaces of these reaction mechanisms. Table 2 also summarizes the thermally corrected energy barrier (at 298 K and 1 atm), the corresponding imaginary frequency, change of enthalpy and Gibbs free energy for the different reaction steps of NO reduction these reaction steps on Al–MoS<sub>2</sub>.

Providing that NO reduction follows the direct mechanism, the adsorbed NO should be first dissociated into N<sub>ads</sub> and O<sub>ads</sub>



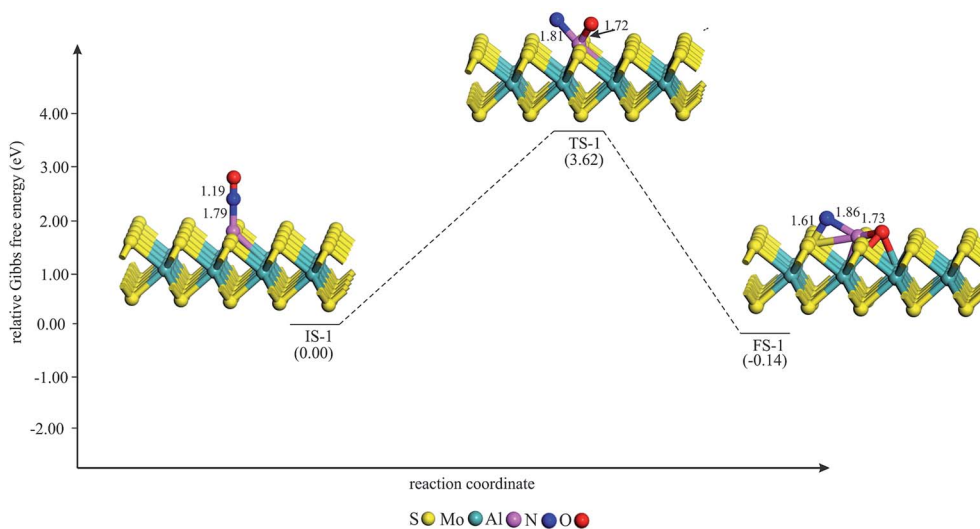


Fig. 3 The Gibbs free energy profile for the dissociation of  $(\text{NO})_2$  moiety on  $\text{Al-MoS}_2$ . All bonds distances are in Å.

species. The Gibbs free energy profile for the dissociation of  $\text{NO}$  is given in Fig. 3. As evident, the most stable adsorption configuration of  $\text{NO}$  (*i.e.*, C1) is adopted as the initial state for

this process (IS-1 in Fig. 3). Next, the bond distance between the N and O atoms increases until the final state FS-1 is achieved. At FS-1, the  $\text{N}_{\text{ads}}$  and  $\text{O}_{\text{ads}}$  moieties are strongly

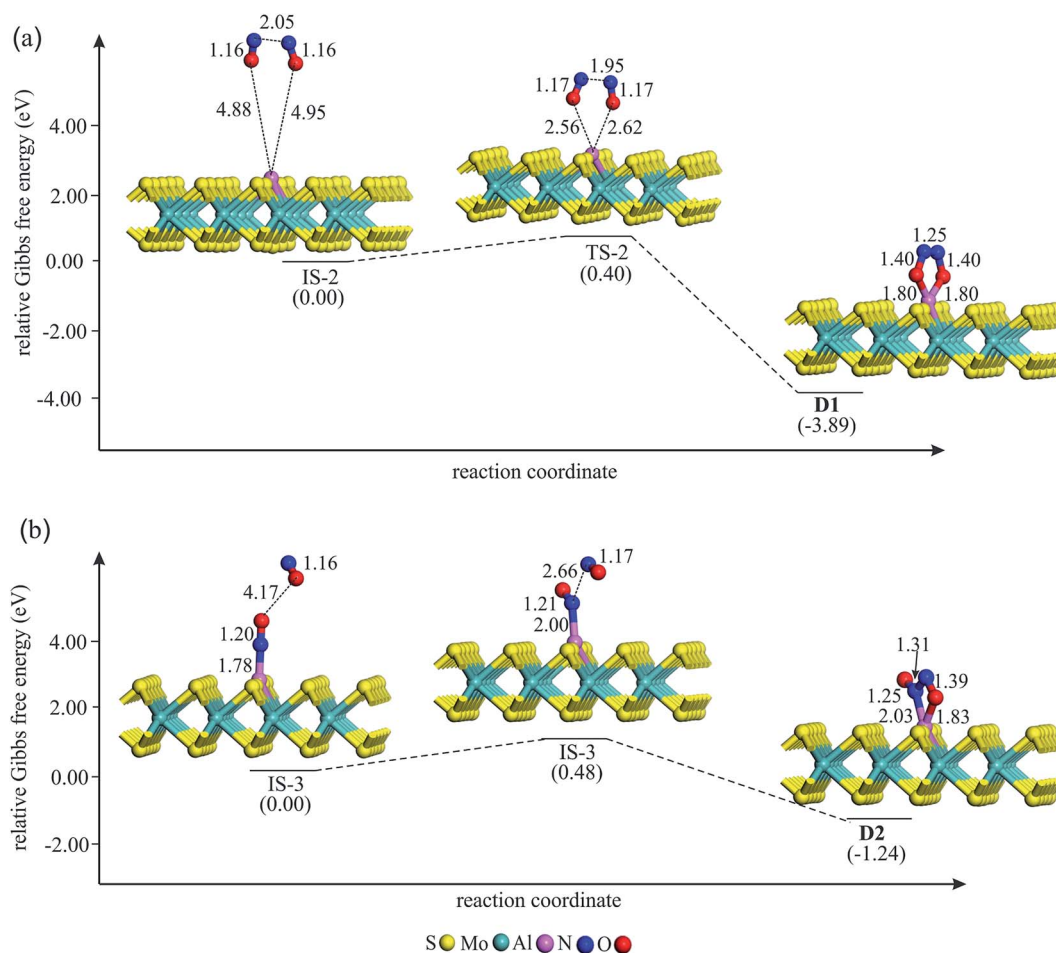


Fig. 4 The Gibbs free energy profile and relaxed stationary points for the coadsorption of  $(\text{NO})_2$  moiety to form (a) D1 and (b) D2 complexes on  $\text{Al-MoS}_2$ . All bonds distances are in Å.



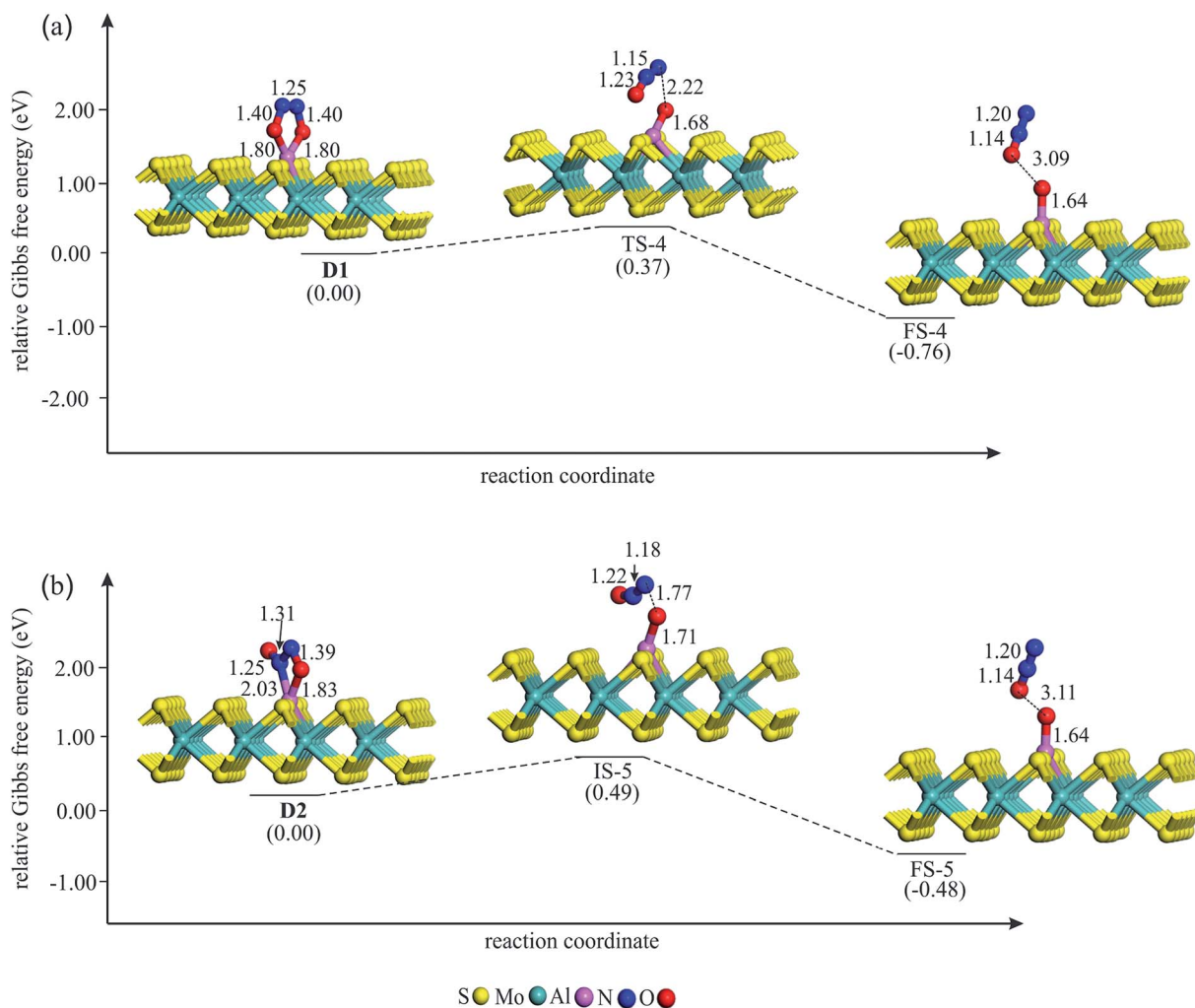


Fig. 5 The Gibbs free energy profile and relaxed stationary points for the dissociation of  $(\text{NO})_2$  on  $\text{Al-MoS}_2$ . All bonds distances are in Å.

chemisorbed between the Mo and S atom of the surface. Owing to the formation of new chemical bonds in FS-1, this process is exothermic by 0.32 eV. In addition, the Gibbs free energy change ( $\Delta G_{298}$ ) for this reaction is negative by 0.14 eV, indicating that it is a thermodynamically favorable process at normal condition (Table 2). However, the large energy barrier (3.62 eV) to reach FS-1 shows that the dissociation of NO cannot be completed at ambient temperature. Therefore, the direct dissociation mechanism is unlikely to happen over the  $\text{Al-MoS}_2$  substrate.

If NO reduction proceeds *via* the dimer mechanism, two NO molecules should be first coadsorbed over the catalyst. Fig. 4 shows the potential energy diagram and corresponding stationary points involved in the formation of coadsorbed NO configurations. After careful structural optimizations, two most stable coadsorbed configurations are found for the NO molecules (configurations **D1** and **D2** in Fig. 4). In both configurations, NO molecules are attached together *via* their N atoms. The optimized N-N bond lengths in **D1** and **D2** are calculated to be 1.25 and 1.31 Å, which are longer than the experimental N-N

bond distance (1.970 Å) in gas phase  $(\text{NO})_2$ .<sup>62</sup> As Fig. 4a indicates,  $(\text{NO})_2$  dimer in **D1** adopts a trapezoid  $\text{O}_{\text{ads}}\text{NNO}_{\text{ads}}$  configuration in which NO molecules are attached to the Al atom through their O-site. From Fig. 4, it is evident that the calculated energy barrier required for the formation of **D1** is only 0.40 eV, which suggests that it can be easily completed at ambient condition. Meanwhile, the change of enthalpy ( $\Delta H_{298}$ ) and Gibbs free energy ( $\Delta G_{298}$ ) is negative by  $-4.48$  and  $-3.89$  eV, respectively, demonstrating that this reaction is exothermic and a thermodynamically favorable process at room temperature (Table 2). From Table 1, it is also seen that about 0.50 |e| shift from the substrate to NO molecules in **D1**, which is largely accumulated over the  $\text{O}_{\text{ads}}$  atoms. Unlike **D1**, NO molecules in **D2** adopt a *trans*  $\text{ON}_{\text{ads}}\text{NO}_{\text{ads}}$  configuration in which the Al-N<sub>ads</sub> and Al-O<sub>ads</sub> bond distances are 2.03 and 1.83 Å, respectively. The coadsorption energy of NO molecules in **D2** is  $-3.55$  eV, which is 1.16 eV smaller (less negative) than that of **D1**. As shown in Fig. 4b, an energy barrier of 0.48 eV should be overcome to reach **D2**, which is larger than the obtained value for **D1**. From Table 2, one can see that the formation of **D2** is



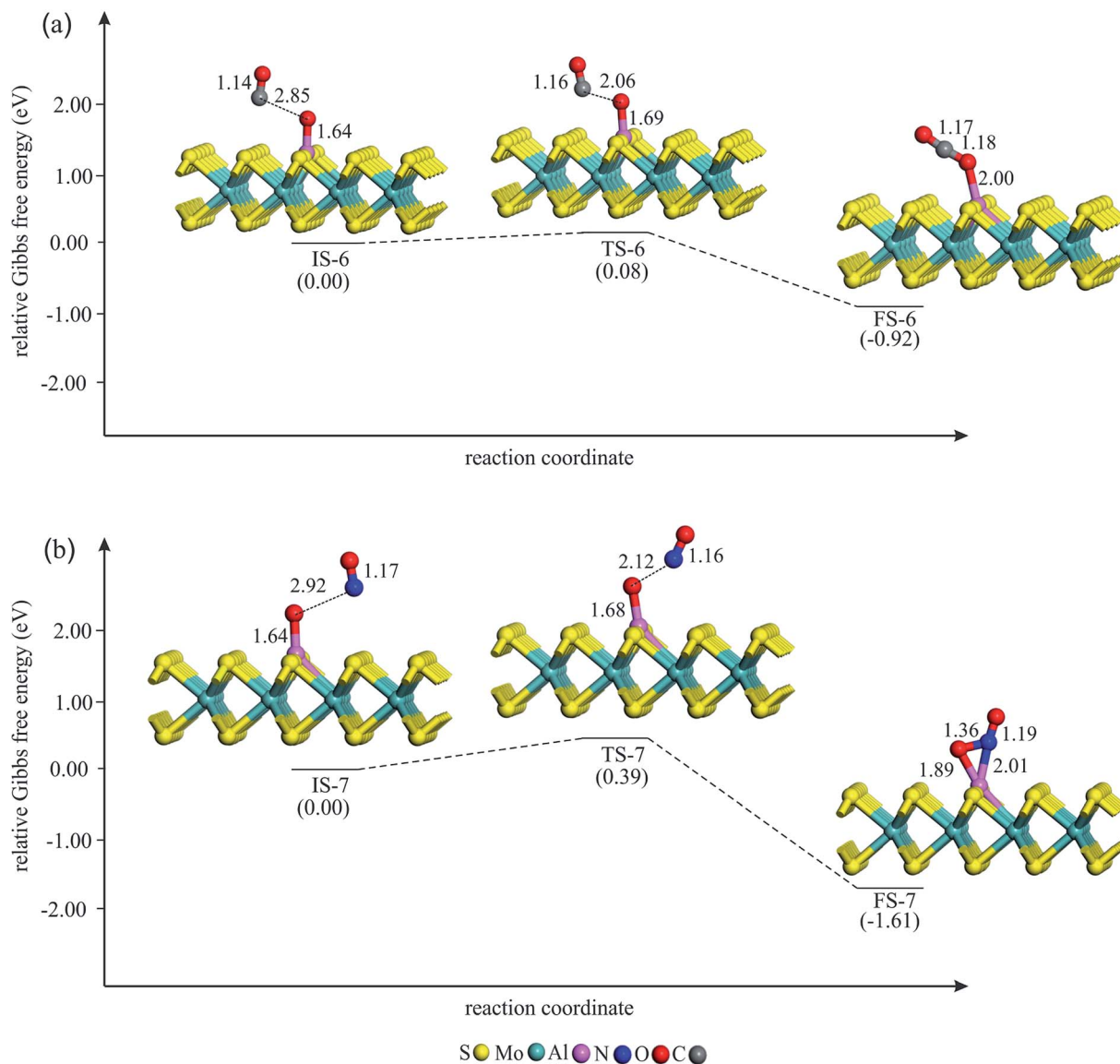


Fig. 6 The Gibbs free energy profile and relaxed stationary points for the removal of  $O_{\text{ads}}$  by (a) CO and (b) NO molecule. All bonds distances are in Å.

**Table 2** Thermally corrected energy barrier ( $E_{\text{bar}}$ , eV) and corresponding imaginary frequency ( $\nu$ ,  $\text{cm}^{-1}$ ), change of enthalpy ( $\Delta H_{298}$ , eV) and change Gibbs free energy ( $\Delta G_{298}$ , eV) values at 1 atm and 298 K for different reaction steps of NO reduction on Al–MoS<sub>2</sub>

Reaction	$E_{\text{bar}}$	$\nu$	$\Delta H_{298}$	$\Delta G_{298}$
IS-1 → FS-1	3.62	786i	−0.32	−0.14
IS-2 → D1	0.40	808i	−4.48	−3.89
IS-3 → D2	0.48	748i	−1.60	−1.24
D1 → FS-4	0.37	692i	−0.62	−0.76
D2 → FS-5	0.49	927i	−0.40	−0.48
IS-6 → FS-6	0.08	826i	−1.26	−0.92
IS-7 → FS-7	0.39	664i	−1.95	−1.61

also accompanied with a large negative  $\Delta H_{298}$  and  $\Delta G_{298}$  values. These results, together with the large coadsorption energies and low energy barriers, indicate that the dimer mechanism should be the most favored pathway to reduce the NO molecules.

In the next step,  $(\text{NO})_2$  moiety is dissociated over Al–MoS<sub>2</sub> to form  $\text{N}_2\text{O}$  and  $\text{O}_{\text{ads}}$  species. Fig. 5 gives the optimized geometry of different stationary points involved in this reaction step. Starting from the coadsorbed NO configurations, one of the N– $\text{O}_{\text{ads}}$  bond of  $(\text{NO})_2$  is elongated until the  $\text{N}_2\text{O}$  and  $\text{O}_{\text{ads}}$  species are formed on the Al–MoS<sub>2</sub> substrate. This leads to 0.12 |e| increase in the positive charge of the Al atom. From Table 2, it is seen that this process is exothermic for both D1 and D2 configurations. The corresponding transition state structures TS-4 and TS-5 are characterized by an imaginary frequency of 692 and 927  $\text{cm}^{-1}$ , respectively, which is related to the cleavage of Al–N, Al–O or N–O bonds. The corresponding energy barrier is calculated to be 0.37 and 0.49 eV, which implies that this reaction step is most likely to complete at normal conditions. We note that these energy barriers are smaller than those reported values over traditional noble metals, like Ag.<sup>4</sup> Finally, the



produced  $\text{N}_2\text{O}$  molecule detaches from the surface owing to its small  $E_{\text{ads}}$  value ( $-0.12$  eV).

In the final step of the reaction, the  $\text{O}_{\text{ads}}$  is removed from the Al atom by interacting with the CO molecule. To this aim, a CO molecule is allowed to approach the  $\text{O}_{\text{ads}}$ . The Gibbs free energy profile for the  $\text{CO} + \text{O}_{\text{ads}} \rightarrow \text{CO}_2$  process is shown in Fig. 6a. The Hirshfeld charge density analysis reveals that about 0.45 electrons transfer from the Al-MoS<sub>2</sub> substrate to the  $\text{O}_{\text{ads}}$ . At IS-6, the C atom of CO is about 2.80 Å away from the  $\text{O}_{\text{ads}}$  and the  $E_{\text{ads}}$  value of CO is obtained to be about  $-0.20$  eV. As CO approaches the  $\text{O}_{\text{ads}}$ , the Al- $\text{O}_{\text{ads}}$  bond distance continually increases and finally  $\text{CO}_2$  molecule is reached on the Al atom. Meanwhile, the atomic charge on the  $\text{O}_{\text{ads}}$  decreases from IS-6 to FS-6. From Table 2, this reaction step is thermodynamically favored ( $\Delta G_{298} = -0.92$  eV) and needs a very small activation energy (0.08 eV). Note that this activation energy is much smaller than the reported value for the removing of the  $\text{O}_{\text{ads}}$  species from Pd (0.91 eV), Ru (1.68 eV) and Pt (0.79 eV) surfaces<sup>63</sup> or transition metal-doped  $\text{C}_2\text{N}$  ( $\approx 0.50$  eV).<sup>64</sup> Also, the energy barrier for the  $\text{CO} + \text{O}_{\text{ads}} \rightarrow \text{CO}_2$  reaction on Al-MoS<sub>2</sub> is smaller than those of reported over Si- (0.29 eV) and Se-doped graphene (0.68 eV),<sup>65</sup> indicating the high catalytic performance of the former system toward the oxidation of CO. Besides, this energy barrier is almost identical with that of reported value by Li and co-workers in the ref. 42. On the other hand, the  $E_{\text{ads}}$  value of  $\text{CO}_2$  is only  $-0.14$  eV, which is less than the proposed value by Deng *et al.* ( $-0.52$  eV)<sup>66</sup> to hinder the poisoning of catalyst at ambient temperature. Thus, the formed  $\text{CO}_2$  molecule detaches from the Al atom and this refreshes the catalyst surface to initiate a new round of the reaction.

One can expect that the  $\text{O}_{\text{ads}}$  may also interact with a NO molecule to produce  $\text{NO}_2$ . The energy profile for this side reaction is given in Fig. 6b. As evident, this reaction step begins with the physisorption of the NO molecule. This leads to the formation of the initial state structure IS-6, in which NO is about 3 Å far from the  $\text{O}_{\text{ads}}$ . Passing the transition state TS-6 with an energy barrier of 0.39 eV, the Al- $\text{O}_{\text{ads}}$  bond breaks and finally  $\text{NO}_2$  molecule is formed on the Al atom. The Hirshfeld analysis indicates that the atomic charge on the  $\text{O}_{\text{ads}}$  decreases from  $-0.45$  to  $-0.18 |e|$  during this reaction step. The produced  $\text{NO}_2$  in FS-6 attaches the Al atom *via* its N atom, with the N-O bonds oriented upwards, like as those other reported studies.<sup>67-70</sup> This process is highly exothermic ( $\Delta H_{298} = -1.95$  eV) and thermodynamically feasible at normal temperature. However, unlike  $\text{CO}_2$ ,  $\text{NO}_2$  is found to interact strongly with the Al atom, and thus blocks the active site of catalyst. However, the larger activation energy of the  $\text{NO} + \text{O}_{\text{ads}} \rightarrow \text{NO}_2$  compared to  $\text{CO} + \text{O}_{\text{ads}} \rightarrow \text{CO}_2$  guaranties that the former reaction should be almost impossible over the Al-MoS<sub>2</sub> substrate.

## 4. Conclusions

Using the first-principles calculations, the reactions pathways and activation energies of NO reduction catalyzed over Al-MoS<sub>2</sub> were investigated. Our computations indicated that the doping of Al atom could greatly tune the surface properties and electronic structure of MoS<sub>2</sub>. The reduction of NO molecules over

Al-MoS<sub>2</sub> follows the dimer mechanism, initiated by the coadsorption of two NO molecules and formation of  $(\text{NO})_2$  moiety on the Al atom. The latter process was found to be exothermic. The subsequent dissociation of  $(\text{NO})_2$  moiety into  $\text{N}_2\text{O}$  and  $\text{O}_{\text{ads}}$  was found to need 0.37 eV activation energies. The  $\text{O}_{\text{ads}}$  is then eliminated by addition of a CO molecule by overcoming a very small activation energy (0.08 eV). These results suggest that Al-MoS<sub>2</sub> may be used as a novel catalyst with high efficiency and stability for reduction of NO molecules.

## Conflicts of interest

The authors declare they have no conflict of interest.

## Acknowledgements

The authors would like to thank the “Computational Center of University of Maragheh” for its technical support of this work.

## References

- 1 A. C. Stern, *Fundamentals of air pollution*, Elsevier, 2014.
- 2 M. Kampa and E. Castanas, *Environ. Pollut.*, 2008, **151**, 362–367.
- 3 Z.-P. Liu and P. Hu, *Top. Catal.*, 2004, **28**, 71–78.
- 4 Z.-P. Liu, S. J. Jenkins and D. A. King, *J. Am. Chem. Soc.*, 2004, **126**, 7336–7340.
- 5 L. Ilieva, G. Pantaleo, I. Ivanov, R. Nedyalkova, A. M. Venezia and D. Andreeva, *Catal. Today*, 2008, **139**, 168–173.
- 6 A. Patel, P. Shukla, T. E. Rufford, V. Rudolph and Z. Zhu, *Chem. Eng. J.*, 2014, **255**, 437–444.
- 7 X. Zhang, Z. Lu, Y. Tang, Z. Fu, D. Ma and Z. Yang, *Phys. Chem. Chem. Phys.*, 2014, **16**, 20561–20569.
- 8 A. Eichler and J. Hafner, *J. Catal.*, 2001, **204**, 118–128.
- 9 Z.-P. Liu and P. Hu, *Top. Catal.*, 2004, **28**, 71–78.
- 10 Z.-P. Liu, S. J. Jenkins and D. A. King, *J. Am. Chem. Soc.*, 2004, **126**, 7336–7340.
- 11 F. Rondinelli, N. Russo and M. Toscano, *J. Chem. Theory Comput.*, 2008, **4**, 1886–1890.
- 12 S. Roy and A. Baiker, *Chem. Rev.*, 2009, **109**, 4054–4091.
- 13 U. Elizundia, D. Duraiswami, B. Pereda-Ayo, R. López-Fonseca and J. R. González-Velasco, *Catal. Today*, 2011, **176**, 324–327.
- 14 W.-C. Ding, X.-K. Gu, H.-Y. Su and W.-X. Li, *J. Phys. Chem. C*, 2014, **118**, 12216–12223.
- 15 K. Thirunavukkarasu, K. Thirumoorthy, J. Libuda and C. S. Gopinath, *J. Phys. Chem. B*, 2005, **109**, 13272–13282.
- 16 Y. Wang, D. Zhang, Z. Yu and C. Liu, *J. Phys. Chem. C*, 2010, **114**, 2711–2716.
- 17 T. Wehling, K. Novoselov, S. Morozov, E. Vdovin, M. Katsnelson, A. Geim and A. Lichtenstein, *Nano Lett.*, 2008, **8**, 173–177.
- 18 Z. Ao, S. Li and Q. Jiang, *Solid State Commun.*, 2010, **150**, 680–683.
- 19 L. Qu, Y. Liu, J.-B. Baek and L. Dai, *ACS Nano*, 2010, **4**, 1321–1326.



- 20 N. Song, Y. Wang, H. Gao, W. Jiang, J. Zhang, B. Xu, Q. Sun and Y. Jia, *Phys. Lett. A*, 2015, **379**, 815–819.
- 21 H. Luo, Y. Cao, J. Zhou, J. Feng, J. Cao and H. Guo, *Chem. Phys. Lett.*, 2016, **643**, 27–33.
- 22 Z. Lu, P. Lv, Y. Liang, D. Ma, Y. Zhang, W. Zhang, X. Yang and Z. Yang, *Phys. Chem. Chem. Phys.*, 2016, **18**, 21865–21870.
- 23 M. D. Esrafil, P. Mousavian and F. A. Rad, *J. Mol. Graphics Modell.*, 2018, **82**, 101–107.
- 24 K. Kakaei, M. D. Esrafil and A. Ehsani, in *Interface Science and Technology*, ed. K. Kakaei, M. D. Esrafil and A. Ehsani, Elsevier, 2019, vol. 27, pp. 387–437.
- 25 A. Splendiani, L. Sun, Y. Zhang, T. Li, J. Kim, C.-Y. Chim, G. Galli and F. Wang, *Nano Lett.*, 2010, **10**, 1271–1275.
- 26 G. Eda, H. Yamaguchi, D. Voiry, T. Fujita, M. Chen and M. Chhowalla, *Nano Lett.*, 2011, **11**, 5111–5116.
- 27 D. Merki and X. Hu, *Energy Environ. Sci.*, 2011, **4**, 3878–3888.
- 28 J. D. Benck, T. R. Hellstern, J. Kibsgaard, P. Chakthranont and T. F. Jaramillo, *ACS Catal.*, 2014, **4**, 3957–3971.
- 29 B. Hinnemann, P. G. Moses, J. Bonde, K. P. Jørgensen, J. H. Nielsen, S. Horch, I. Chorkendorff and J. K. Nørskov, *J. Am. Chem. Soc.*, 2005, **127**, 5308–5309.
- 30 Y. Yin, J. Han, Y. Zhang, X. Zhang, P. Xu, Q. Yuan, L. Samad, X. Wang, Y. Wang and Z. Zhang, *J. Am. Chem. Soc.*, 2016, **138**, 7965–7972.
- 31 H. Li, M. Du, M. J. Mleczko, A. L. Koh, Y. Nishi, E. Pop, A. J. Bard and X. Zheng, *J. Am. Chem. Soc.*, 2016, **138**, 5123–5129.
- 32 C. González, B. Biel and Y. J. Dappe, *Phys. Chem. Chem. Phys.*, 2017, **19**, 9485–9499.
- 33 K. Zhang, S. Feng, J. Wang, A. Azcatl, N. Lu, R. Addou, N. Wang, C. Zhou, J. Lerach and V. Bojan, *Nano Lett.*, 2015, **15**, 6586–6591.
- 34 D. Ma, W. Ju, T. Li, X. Zhang, C. He, B. Ma, Z. Lu and Z. Yang, *Appl. Surf. Sci.*, 2016, **383**, 98–105.
- 35 D. Ma, W. Ju, T. Li, G. Yang, C. He, B. Ma, Y. Tang, Z. Lu and Z. Yang, *Appl. Surf. Sci.*, 2016, **371**, 180–188.
- 36 D. Mombrú, R. Faccio and Á. W. Mombrú, *Appl. Surf. Sci.*, 2018, **462**, 409–416.
- 37 X. Dai, K. Du, Z. Li, M. Liu, Y. Ma, H. Sun, X. Zhang and Y. Yang, *ACS Appl. Mater. Interfaces*, 2015, **7**, 27242–27253.
- 38 Y. C. Lin, D. O. Dumcenco, H. P. Komsa, Y. Niimi, A. V. Krasheninnikov, Y. S. Huang and K. Suenaga, *Adv. Mater.*, 2014, **26**, 2857–2861.
- 39 D. Ma, Y. Tang, G. Yang, J. Zeng, C. He and Z. Lu, *Appl. Surf. Sci.*, 2015, **328**, 71–77.
- 40 B. Xiao, P. Zhang, L. Han and Z. Wen, *Appl. Surf. Sci.*, 2015, **354**, 221–228.
- 41 S. Park, J. Park, H. Abroshan, L. Zhang, J. K. Kim, J. Zhang, J. Guo, S. Siahrostami and X. Zheng, *ACS Energy Lett.*, 2018, **3**, 2685–2693.
- 42 D. Li, W. Li and J. Zhang, *Appl. Surf. Sci.*, 2019, **484**, 1297–1303.
- 43 R. Addou, L. Colombo and R. M. Wallace, *ACS Appl. Mater. Interfaces*, 2015, **7**, 11921–11929.
- 44 M. Houssa, K. Iordanidou, G. Pourtois, V. Afanas'ev and A. Stesmans, *Appl. Surf. Sci.*, 2017, **416**, 853–857.
- 45 L.-p. Feng, J. Su, S. Chen and Z.-t. Liu, *Mater. Chem. Phys.*, 2014, **148**, 5–9.
- 46 H. Li, C. Tsai, A. L. Koh, L. Cai, A. W. Contryman, A. H. Fragapane, J. Zhao, H. S. Han, H. C. Manoharan and F. Abild-Pedersen, *Nat. Mater.*, 2016, **15**, 48.
- 47 H.-P. Komsa, S. Kurasch, O. Lehtinen, U. Kaiser and A. V. Krasheninnikov, *Phys. Rev. B: Condens. Matter Mater. Phys.*, 2013, **88**, 035301.
- 48 S. Kretschmer, H.-P. Komsa, P. Bøggild and A. V. Krasheninnikov, *J. Phys. Chem. Lett.*, 2017, **8**, 3061–3067.
- 49 C. Ataca and S. Ciraci, *Phys. Rev. B: Condens. Matter Mater. Phys.*, 2012, **85**, 195410.
- 50 B. Delley, *J. Chem. Phys.*, 1990, **92**, 508–517.
- 51 B. Delley, *J. Chem. Phys.*, 2000, **113**, 7756–7764.
- 52 J. P. Perdew, K. Burke and M. Ernzerhof, *Phys. Rev. Lett.*, 1996, **77**, 3865–3868.
- 53 B. Delley, *Phys. Rev. B: Condens. Matter Mater. Phys.*, 2002, **66**, 155125.
- 54 S. Grimme, *J. Comput. Chem.*, 2004, **25**, 1463–1473.
- 55 S. Grimme, *J. Comput. Chem.*, 2006, **27**, 1787–1799.
- 56 Y. Jing, X. Tan, Z. Zhou and P. Shen, *J. Mater. Chem. A*, 2014, **2**, 16892–16897.
- 57 A. Basak, D. Das, D. Sen and K. Chattopadhyay, *Comput. Mater. Sci.*, 2014, **95**, 399–407.
- 58 C. Kittel, P. McEuen and P. McEuen, *Introduction to Solid State Physics*, Wiley New York, 1996.
- 59 Y. Xie, Y.-P. Huo and J.-M. Zhang, *Appl. Surf. Sci.*, 2012, **258**, 6391–6397.
- 60 M. D. Esrafil, *Chem. Phys. Lett.*, 2018, **695**, 131–137.
- 61 Y. Chen, Y.-j. Liu, H.-x. Wang, J.-x. Zhao, Q.-h. Cai, X.-z. Wang and Y.-h. Ding, *ACS Appl. Mater. Interfaces*, 2013, **5**, 5994–6000.
- 62 C. E. Dinerman and G. E. Ewing, *J. Chem. Phys.*, 1970, **53**, 626–631.
- 63 X.-Q. Gong, Z.-P. Liu, R. Raval and P. Hu, *J. Am. Chem. Soc.*, 2004, **126**, 8–9.
- 64 D. W. Ma, Q. Wang, X. Yan, X. Zhang, C. He, D. Zhou, Y. Tang, Z. Lu and Z. Yang, *Carbon*, 2016, **105**, 463–473.
- 65 R. Gholizadeh and Y.-X. Yu, *Appl. Surf. Sci.*, 2015, **357**, 1187–1195.
- 66 Q. Deng, L. Zhao, X. Gao, M. Zhang, Y. Luo and Y. Zhao, *Small*, 2013, **9**, 3506–3513.
- 67 Y.-H. Zhang, Y.-B. Chen, K.-G. Zhou, C.-H. Liu, J. Zeng, H.-L. Zhang and Y. Peng, *Nanotechnology*, 2009, **20**, 185504.
- 68 J. Dai, J. Yuan and P. Giannozzi, *Appl. Phys. Lett.*, 2009, **95**, 232105.
- 69 R. Lv, G. Chen, Q. Li, A. McCreary, A. Botello-Méndez, S. Morozov, L. Liang, X. Declerck, N. Perea-López and D. A. Cullen, *Proc. Natl. Acad. Sci. U. S. A.*, 2015, **112**, 14527–14532.
- 70 Z. Xie, X. Zuo, G.-P. Zhang, Z.-L. Li and C.-K. Wang, *Chem. Phys. Lett.*, 2016, **657**, 18–25.

